Supplementary information

Full-scale aerobic granular sludge for municipal wastewater treatment – granule formation, microbial succession, and process performance

Jennifer Ekholm [a]*, Frank Persson [a], Mark de Blois [b], Oskar Modin [a], Mario Pronk [c,d], Mark C.M. van Loosdrecht [c], Carolina Suarez [e], David J.I. Gustavsson [f,g], Britt-Marie Wilén [a]

[a] Chalmers University of Technology, Department of Architecture and Civil Engineering, Sven Hultins gata 6, 412 96 Gothenburg, Sweden

[b] H2OLAND, Östra Vattugränd 2, 441 30 Alingsås, Sweden

[c] Department of Biotechnology, Delft University of Technology, Van der Maasweg 9, 2629 HZ Delft, The Netherlands

[d] Royal HaskoningDHV, Laan 1914 35, 3800 AL Amersfoort, The Netherlands

[e] Division of Water Resources Engineering, Faculty of Engineering LTH, Lund University, John Ericssons väg 1, 221 00 Lund, Sweden

[f] VA SYD, P.O. Box 191, 201 21 Malmö, Sweden

[g]Sweden Water Research, Scheelevägen 15, 223 70 Lund, Sweden

* Corresponding author. Email: jennifer.ekholm@chalmers.se

Supplementary description of the technical challenges

The inflow to the AGS reactors was not regulated by a flowmeter until the 19th of September 2018, leading to an uncertainty of the up-flow velocity, which could have affected the start-up time. Also, the prediction model did not work properly, it started the next cycle earlier than needed when the inflow buffer tank was only partially filled, giving the reactor too low flow.

Online measurement of nitrate, suspended solids, total solids and sludge level in the reactors did not work properly for longer periods of time. As the process control is based on ammonium concentration in the reactor, the lack of nitrate concentration data was not a problem, although the nitrate concentration could have helped the denitrification operation control. The ammonium analyser was from time to time out of order. In those cases, the aeration phase was instead controlled solely on time, instead of ending the aeration when the concentration of ammonium had decreased to a specific level. Another challenge during the start-up was the lack of personnel to fully perform the extensive sampling and measurement program.

Another challenge during the start-up was that the CAS was, as planned, disconnected from October 2018 to July 2019, leading to increased flow- and mass load to the AGS reactors. During the reconstruction of the plant, a temporary sludge handling process was put in practice, but the control system was programmed according to the future sludge handling process. The system was malfunctioning, and the sludge storage became full, leading to circulation of sludge between the sludge storage and pre-settlers. This had implication for the AGS process as the sludge discharge, with purpose to remove less well settling sludge, was recirculated back into the pre-settler and fed to

the AGS reactors (negative seeding). After the start-up of the CAS the plant had problem with an occasional inflow from the CAS into the feed buffer of the AGS plant, especially in July 2019.

Another problem was that the programming of the operation system did not allow for a waiting time for the sludge to settle before the sludge discharge. The discharge was done in each cycle directly after the feeding, when the sludge bed was expanded. If there was less well-settling sludge in the reactor, this led to a larger mass of sludge withdrawal as much sludge was located by the discharge outlet. Also, if the sludge in the reactor had a floccular part which was to a large extent located over the discharge outflow, not all floccular sludge was removed in the sludge discharge, leaving the "worst" floccular sludge to stay in the reactor. If the sludge bed would have been allowed to settle a short time, the most upper part of the sludge bed, i.e. floccular sludge, could have been removed.

Another technical failure was a sludge discharge valve that unforeseen was open and leaked sludge from R1, probably from the start until 21st August 2019. The sludge leakage was noticed when the level in the AGS-sludge buffer tank slowly increased, which should have increased its level only at sludge discharge operation.

Supplementary details on amplicon sequencing

DNA was extracted according to the manufacturer's instructions, with dual runs in the FastPrep-24 at settings 6 m/s for 40 seconds, with cooling at 4 °C between the runs. The concentration of the DNA was measured using a Qubit 3.0 fluorometer (Thermo Fisher Scientific).

PCR was carried out with dual indexing (Kozich et al. 2013) of the primers. PCR was conducted in 40 µL reactions with 0.4 µL Phusion Hot Start II DNA Polymerase (Thermo Fisher Scientific), 5X Phusion HF Buffer (8 µL), 10 mM dNTPs (0.8 µL), 40 ng of template DNA, and primers (10 µM, 2 µL each). The following PCR program was used: activation at 98 °C for 30 seconds, denaturation at 98 °C for 10 seconds, annealing at 55.8 °C for 30 seconds, and extension at 72 °C for 30 seconds for 30 cycles, and final elongation at 72 °C for 10 minutes.

PCR products were purified with MagJet NGS Cleanup and Size Selection Kit (Thermo Fisher Scientific). Purified PCR products were pooled in equimolar amounts based on DNA concentration measurements using the Qubit 3.0. Quality control of the pool was carried out using TapeStation (Agilent Technologies). Sequencing was conducted in dual runs on a MiSeq (2×300) using reagent kit V3 (Illumina) with spiking of phiX at 10%.

Supplementary Tables

Table S1. Typical cycle operation of the AGS plant at dry- and rain weather flow.

Phase	**Dry weather flow (min)**	**Rain weather flow (min)**
Fill/decant	52	59
Sludge discharge	3	2
Pulse aeration pre-DN (not every cycle)	19	7
Aeration	121	32
Pulse aeration post-DN	86	12
Settling	32	30
Total time	313	141

Table S2. Design and measured influent composition.

	Design		**Measured**	
Parameter/time period	Jul-Aug (kg/d)	Other months (kg/d)	Jul-Aug (kg/d)	Other months (kg/d)
COD	1596	938	672 ± 81	570 ± 27
BOD_7	727	410	331 ± 38	264 ± 7
Total Kjeldahl-nitrogen (TKN)	198	108	134 ± 41	97 ± 27
TP	20	11	12 ± 3	9 ± 2
BOD_7/TKN	> 3	> 3	3 ± 1 *	3 ± 1 *

* See Table 1 for more detailed information.

Table S3. Probes for fluorescence in situ hybridisation.

Probe	**Target**	**Figures**	**References**
DAPI	DNA/poly-P	Figure S15 and S16	
PAO651 (Cy3)	Ca. *Accumulibacter*	Figure S16 B and D	Crocetti et al. 2000 [1]
Tetra183 + Tetra617 (FAM)	*Tetrasphaera*	Figure S16 A and C	Dueholm et al. 2020 [2]
CPB_654 (Cy3)	*Competibacter*	Figure S16 A and C	McIlroy et al. 2015 [3]
Dechlo2 (Cy5)	*Dechloromonas*	Figure S16 B and D	Sanguin et al. 2005 [4]
SYTO40	DNA + RNA	Figure S15 and S15	
AOB-mix (Cy3)	*Nitrosomonas*	Figure S15 A and B	Lukumbuzya et al. 2020 [5]
Ntoga122 (FAM)	*Ca*. Nitrotoga	Figure S15 A and B	Lücker et al. 2015 [6]
Nspa662 (Cy5)	*Nitrospira*	Figure S15 A and B	Daims et al. 2001 [7]
NLIMI91 (Cy3)	*Trichococcus*	Figure S15 C and D	Liu and Seviour 2001 [8]

Table S4. Effluent concentrations (mg/L) from the AGS plant. Data show averages ± st. dev. during the study period (July 2018 - Oct 2019).

Reactor	**BOD_7**	**COD**	**COD filtered**	**TP**	**PO_4^{3-}-P**	**TKN**	**NH_4^+-N**	**NO_3^--N**	**NO_2^--N**	**SS**	**pH**
R1	6.9 ± 3.3	50.7 ± 20.9	42.6 ± 16.4	1.7 ± 1.1	1.4 ± 1.1	10.3 ± 10.1	5.2 ± 8.1	8.1 ± 8.0	0.3 ± 0.4	10.4 ± 4.5	7.1 ± 0.3
R2	6.1 ± 2.5	49.5 ± 21.3	39.6 ± 12.6	2.0 ± 2.1	1.7 ± 1.8	7.4 ± 6.8	3.6 ± 5.5	9.5 ± 7.1	0.3 ± 0.3	10.8 ± 6.0	7.0 ± 0.3
AGS-plant	6.5 ± 2.9	50.1 ± 21.1	41.1 ± 14.5	1.8 ± 1.6	1.5 ± 1.5	8.8 ± 8.4	4.4 ± 6.8	8.8 ± 7.6	0.3 ± 0.3	10.6 ± 5.3	7.1 ± 0.3

Supplementary Figures

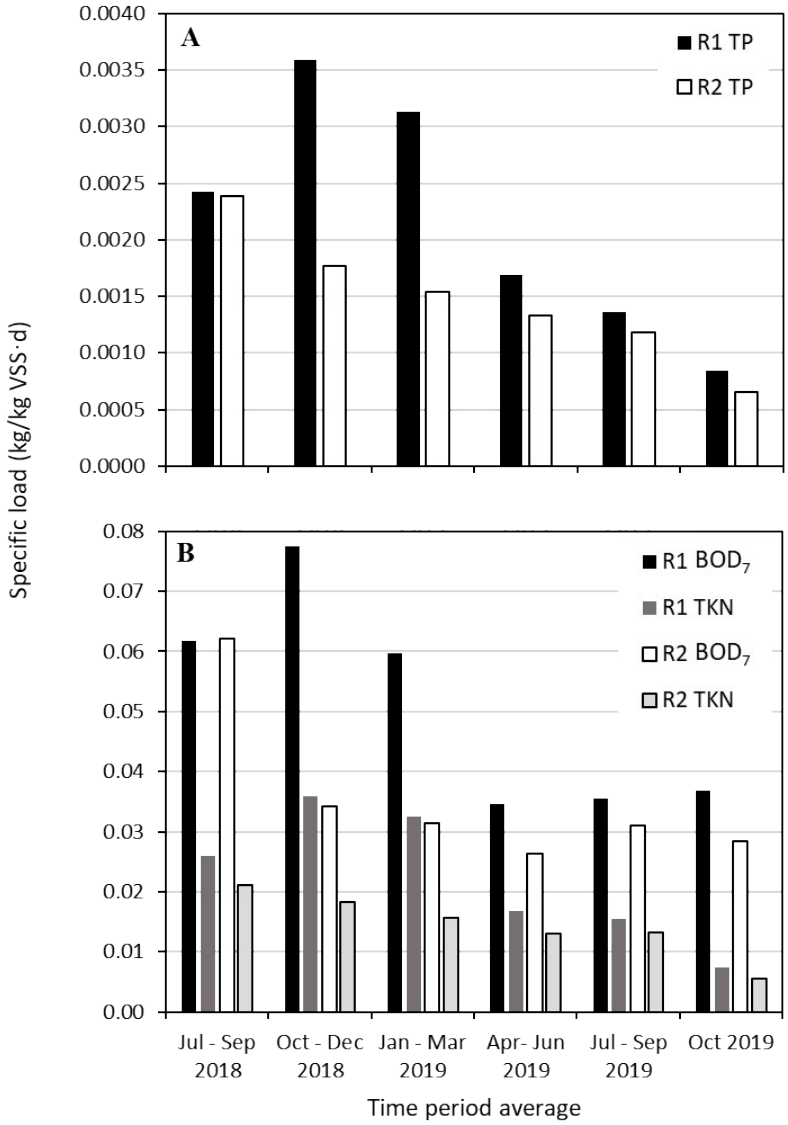

Figure S1. Specific loads of TP (A) and BOD_7, TKN (B) to R1 and R2.

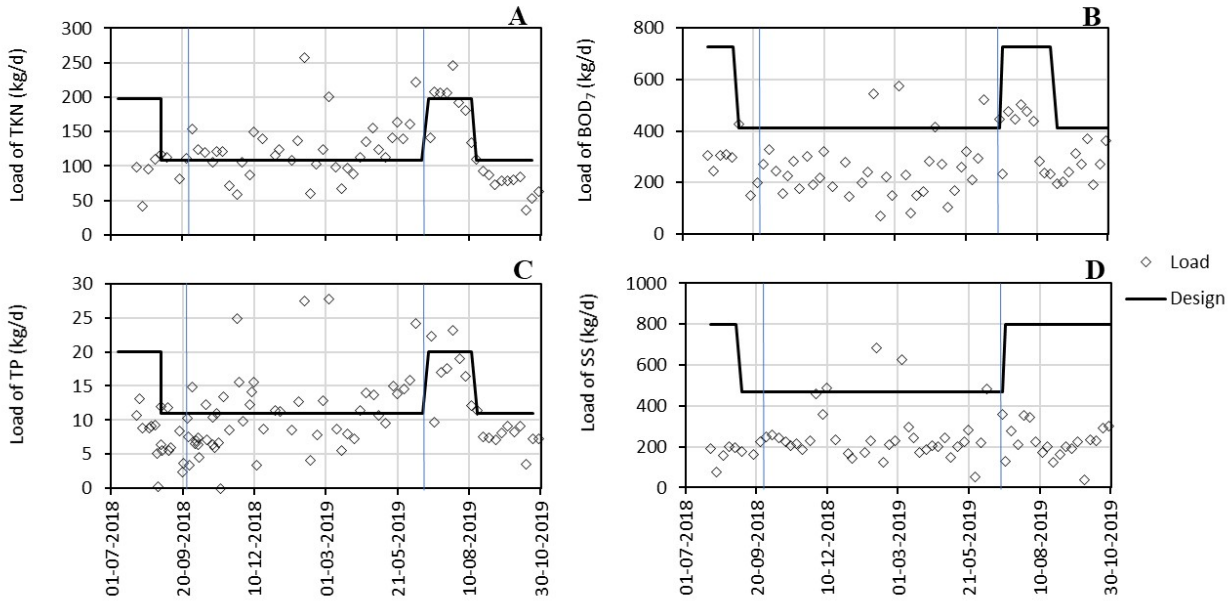

Figure S2. Load and design load of TKN (A), BOD_7 (B), TP (C) and SS (D) in the influent to the AGS plant.

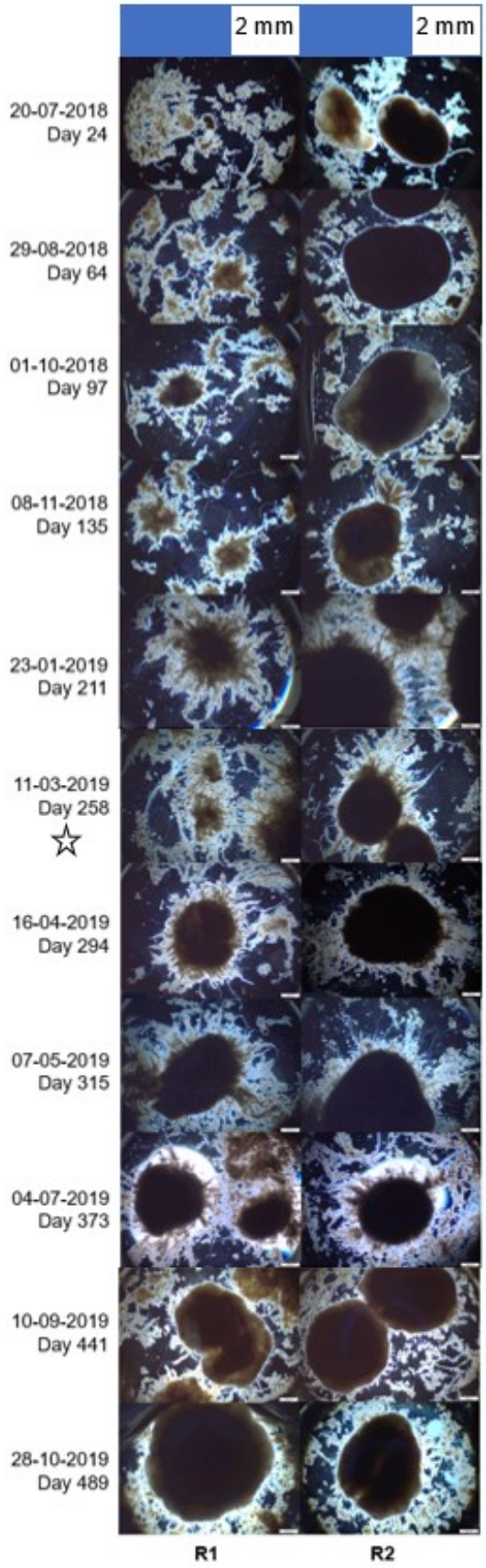

Figure S3. Microscopic images of the granular sludge over time. The scale bars designate 2 mm. The star represents the time of reseeding of R1.

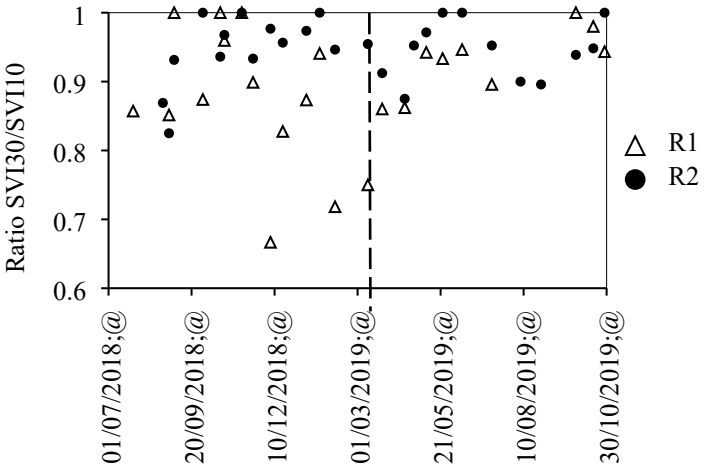

Figure S4. Ratio of SVI_{30} and SVI_{10} for R1 and R2. The dashed line marks reseeding of R1.

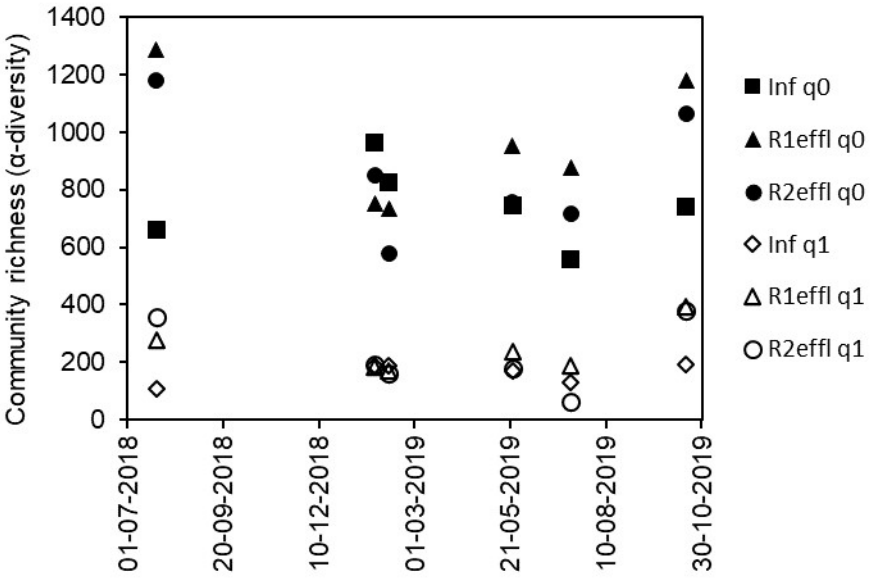

Figure S5. Dynamics in alpha diversity at q=0 (richness) over time of the microbial communities in the reactors, influent and effluent.

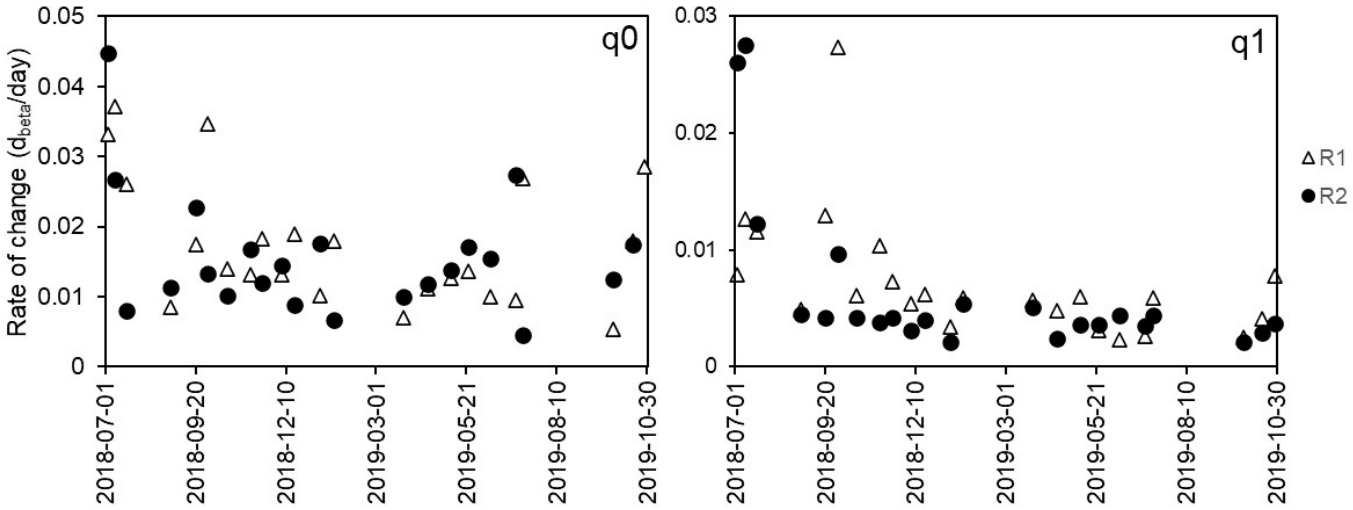

Figure S6. Rate of change in microbial community composition as dissimilarity divided by elapsed time between consecutive sampling days at q=0 (left) and q=1 (right).

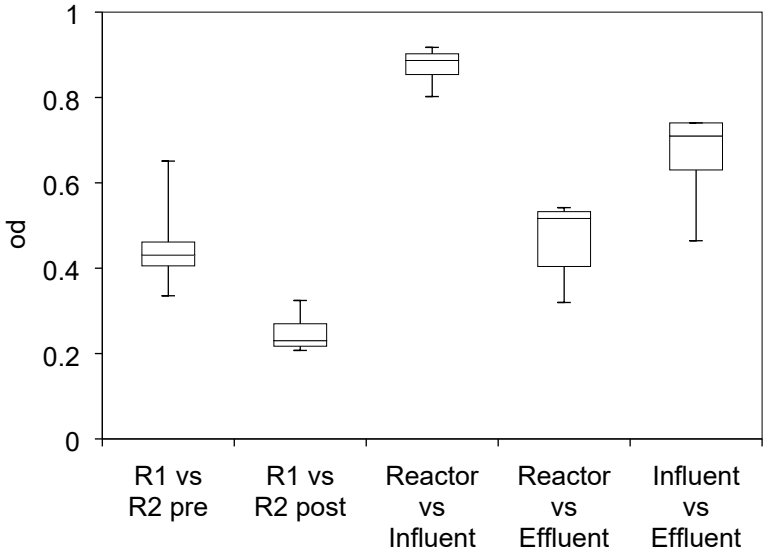

Figure S7. Boxplot of the microbial community dissimilarity (q=0). From left to right: dissimilarity between samples in R1 versus R2 pre reseeding, R1 versus R2 post reseeding, reactors versus influent, reactors versus effluent and influent versus effluent.

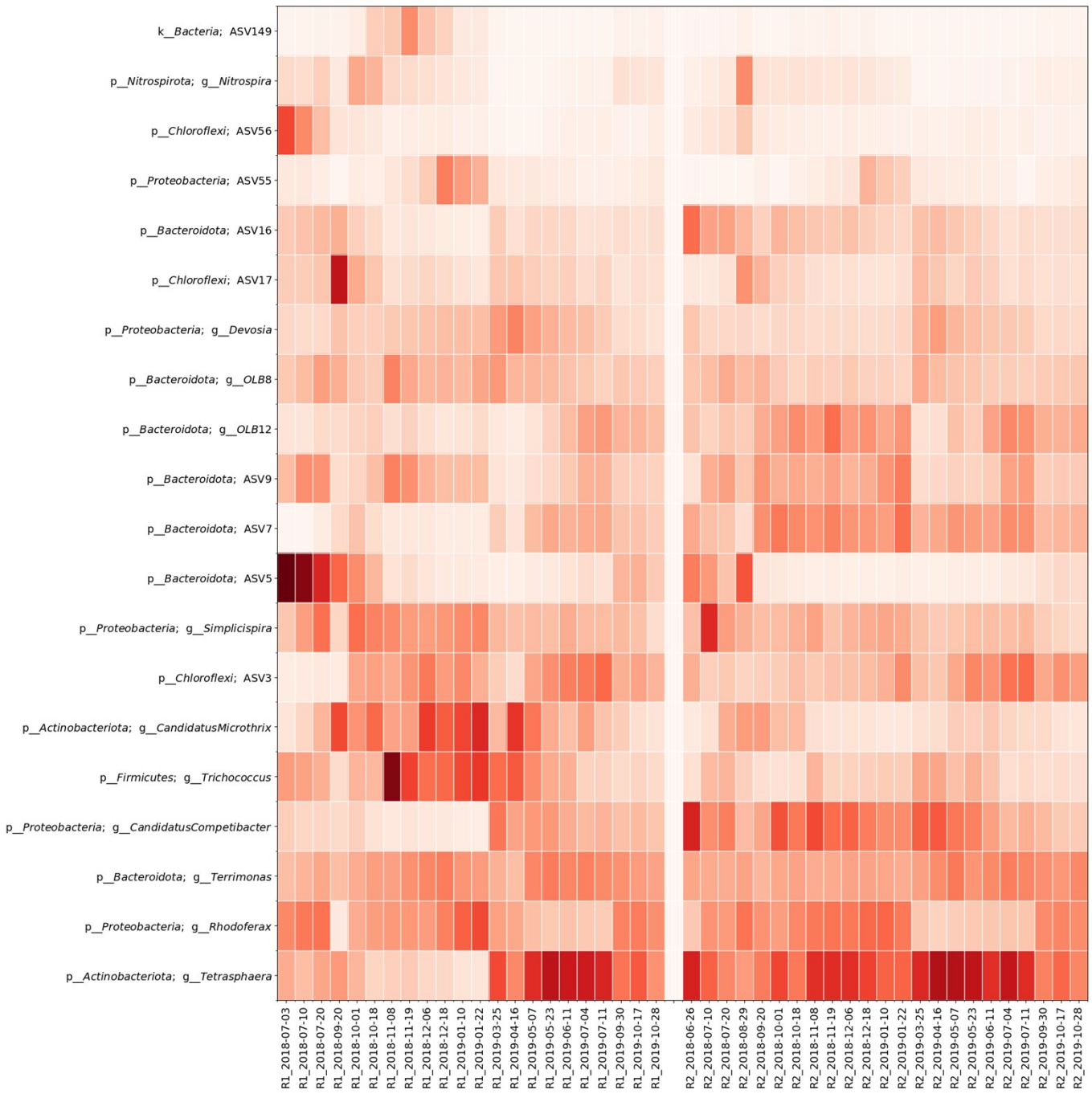

Figure S8. Heatmap of the 20 most abundant genera in R1 and R2 over time. Darker red colour indicates higher abundance.

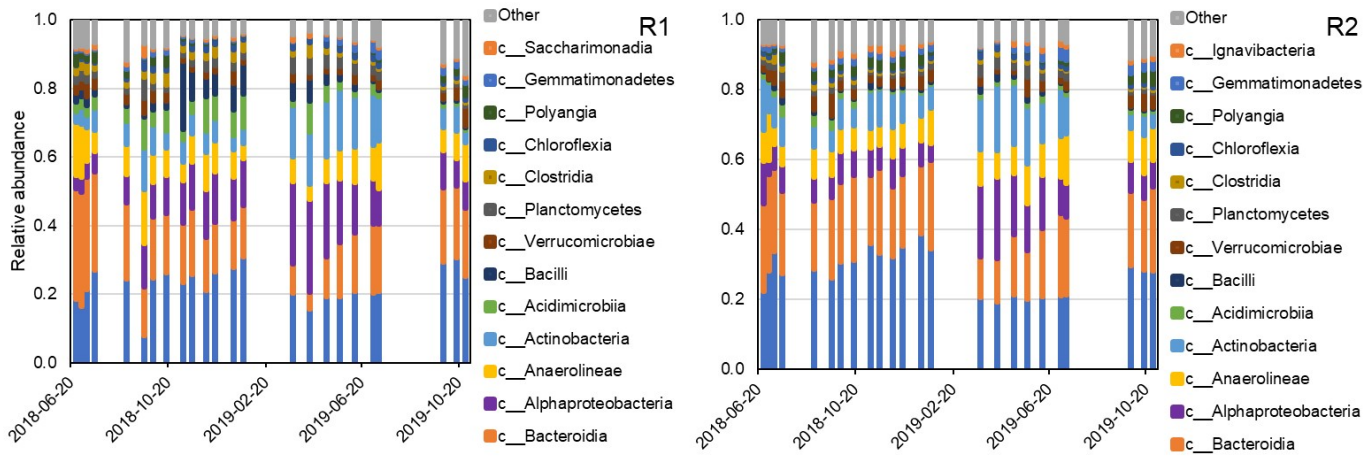

Figure S9. Dynamics in relative abundance of class taxa over time in R1 (left) and R2 (right).

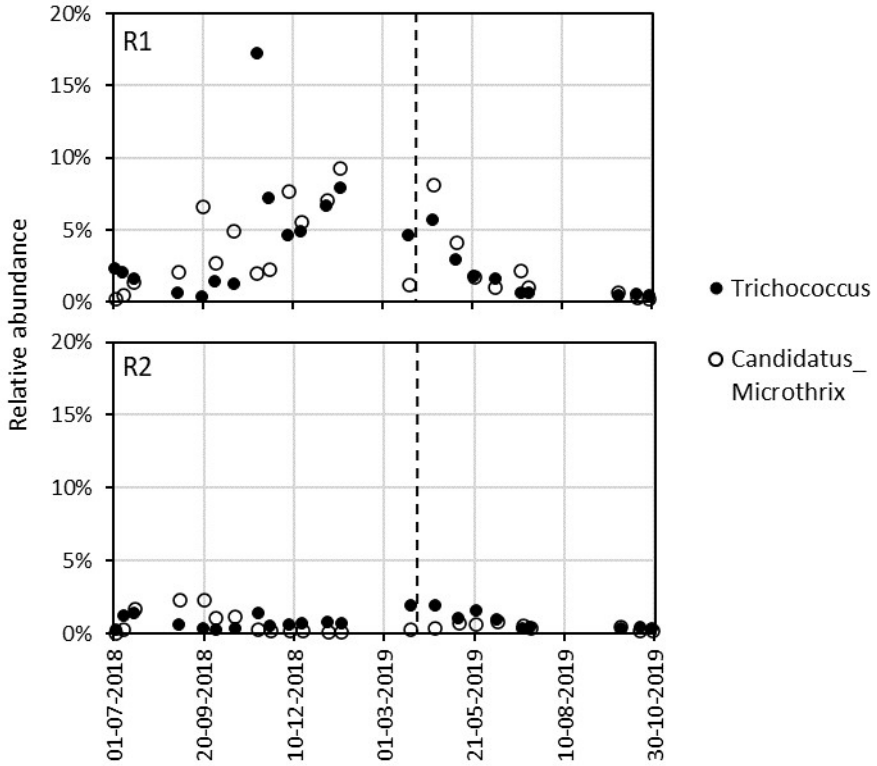

Figure S10. Relative abundance of *Trichococcus* and *Ca*. Microthrix in R1 and R2 over time.

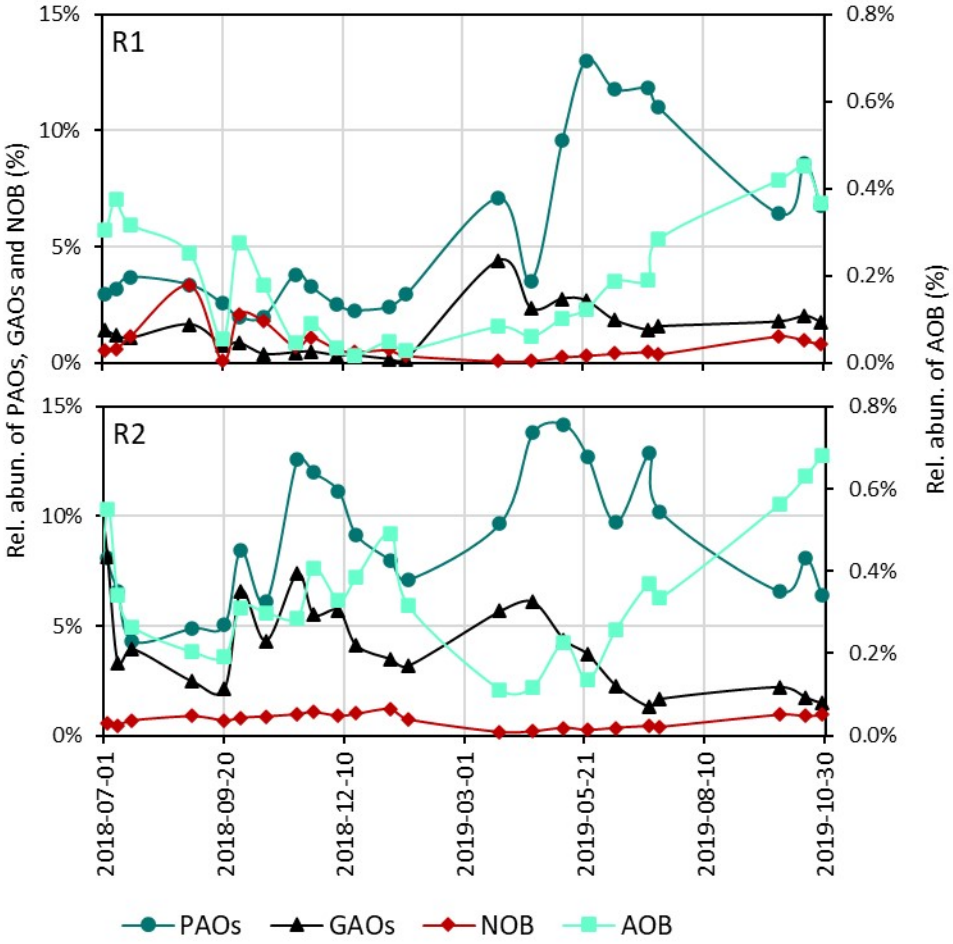

Figure S11. Relative abundance of the key functional groups PAOs, GAOs, NOB and AOB in R1 and R2.

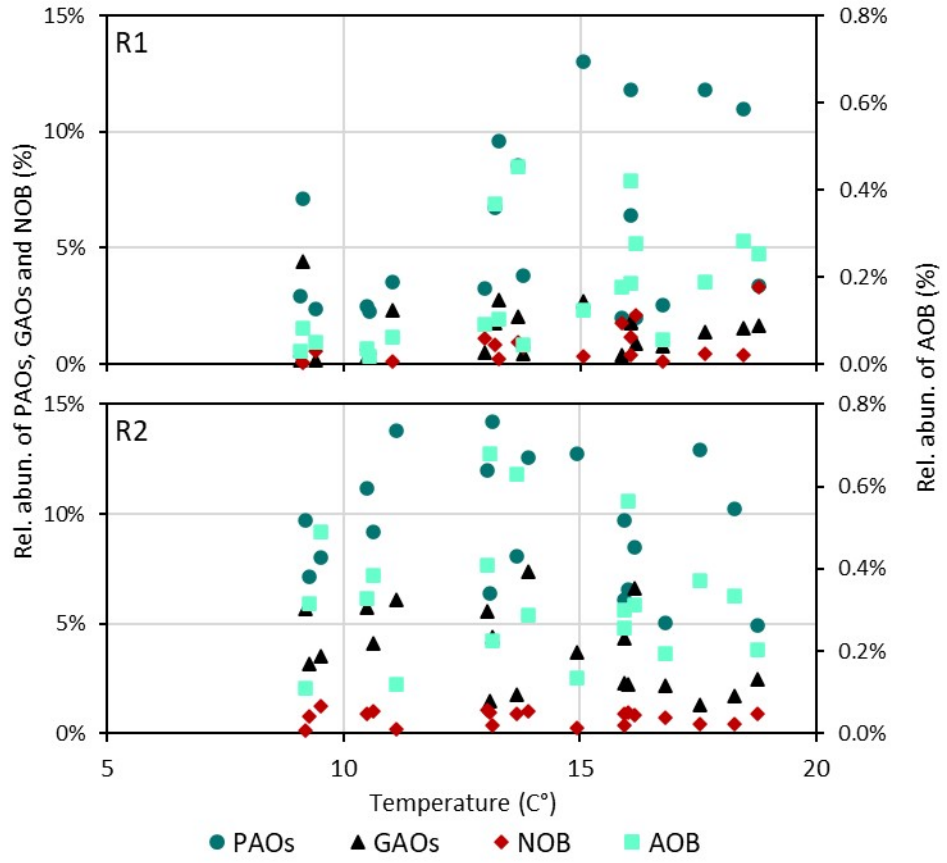

Figure S12. Relative abundance of the key functional groups PAOs, GAOs, NOB and AOB as a function of temperature.

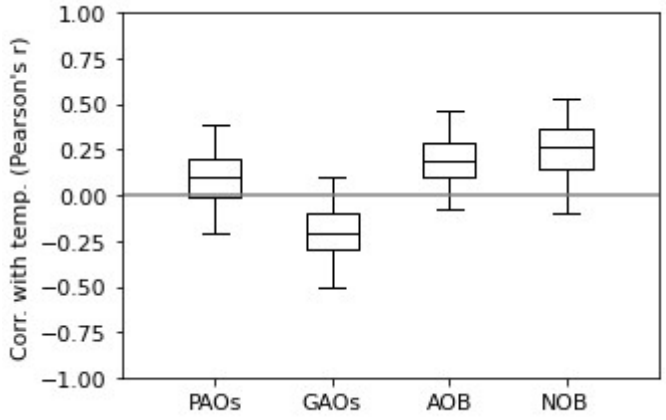

Figure S13. Correlation between the relative abundance of key functional groups and temperature. A distribution of correlation coefficients was calculated using bootstrapping [9]. The dataset with temperature and relative abundances of the functional groups was resampled with replacement 1000 times. For each sample, Pearson's r between temperature and each functional group was calculated. The box plot shows the distribution of r values. The box shows the median and quartiles. The whiskers show the 95% confidence interval. Since r=0 is within the 95%-confidence interval for all functional group, there is no statistically significant correlation at a significance level of 0.05.

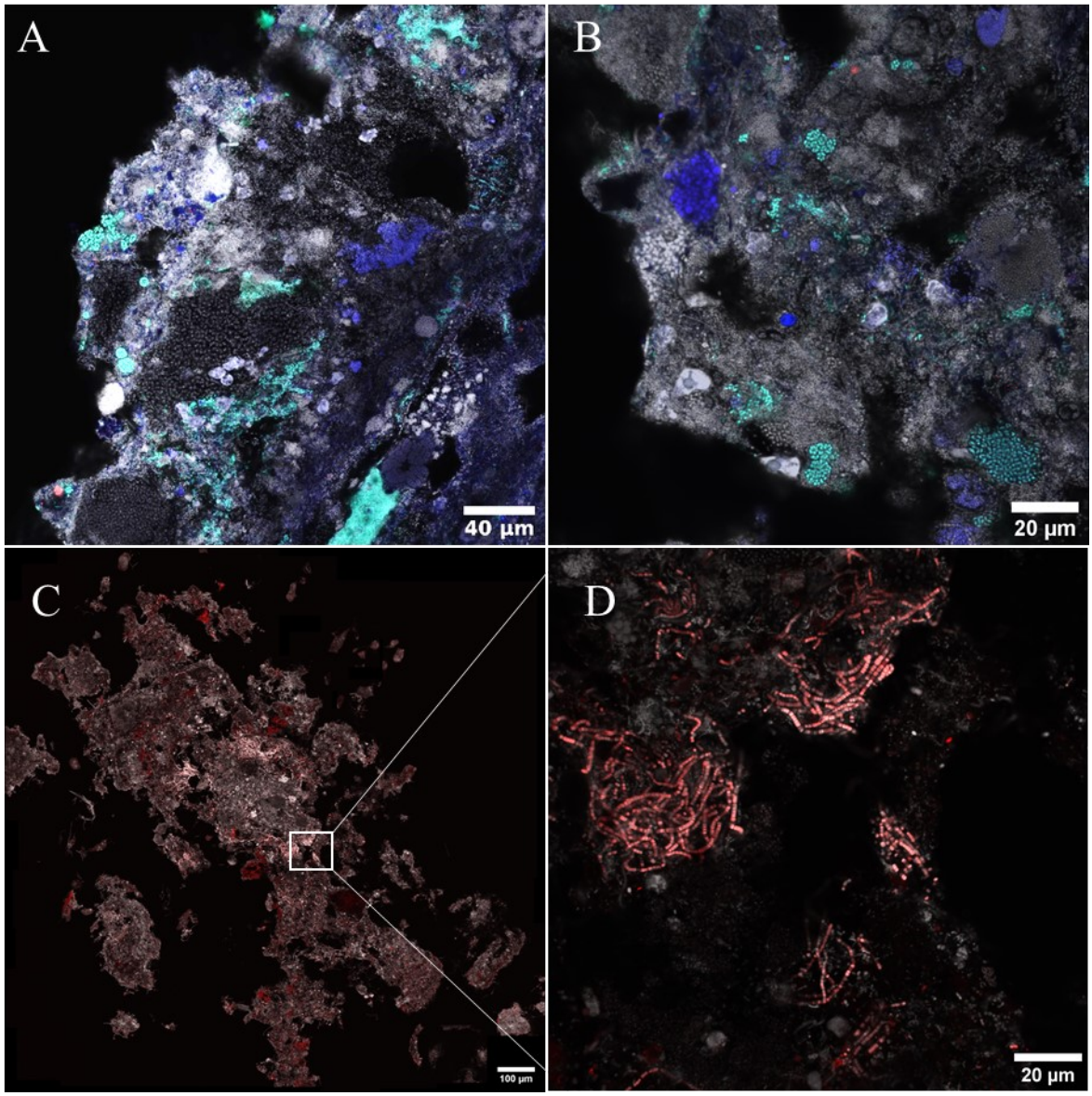

Figure S14. Fluorescence in situ hybridization of granule cryosections. A-B) granules from R2 (October 2019), showing *Nitrosomonas* (cyan), *Ca.* Nitrotoga (blue), and *Nitrospira* (red). C-D) granule from R1 (December 2018) showing filamentous bacteria within *Trichococcus* (red). In all images, biomass (DNA and RNA) is displayed in grey.

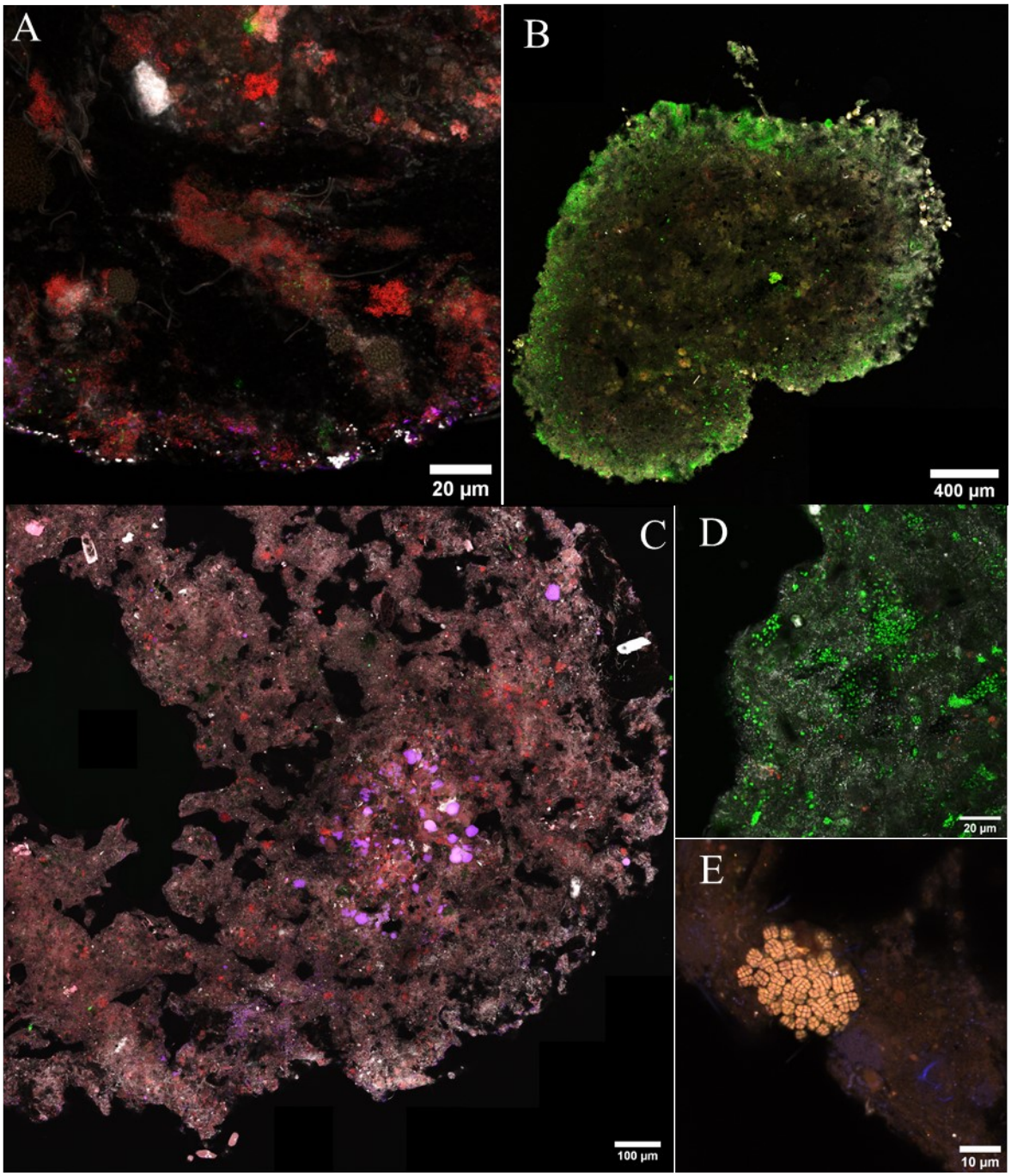

Figure S15. Fluorescence in situ hybridization images of granule cryosections from R2 (October 2019). A, C) showing *Tetrasphaera* (red), *Competibacter* (purple) and *Dechloromonas* (green). B, D) *Ca* Accumulibacter (green) and *Dechloromonas* (red). Poly-P in *Tetrasphaera* (E). In all images, biomass (DNA and RNA) is displayed in grey.

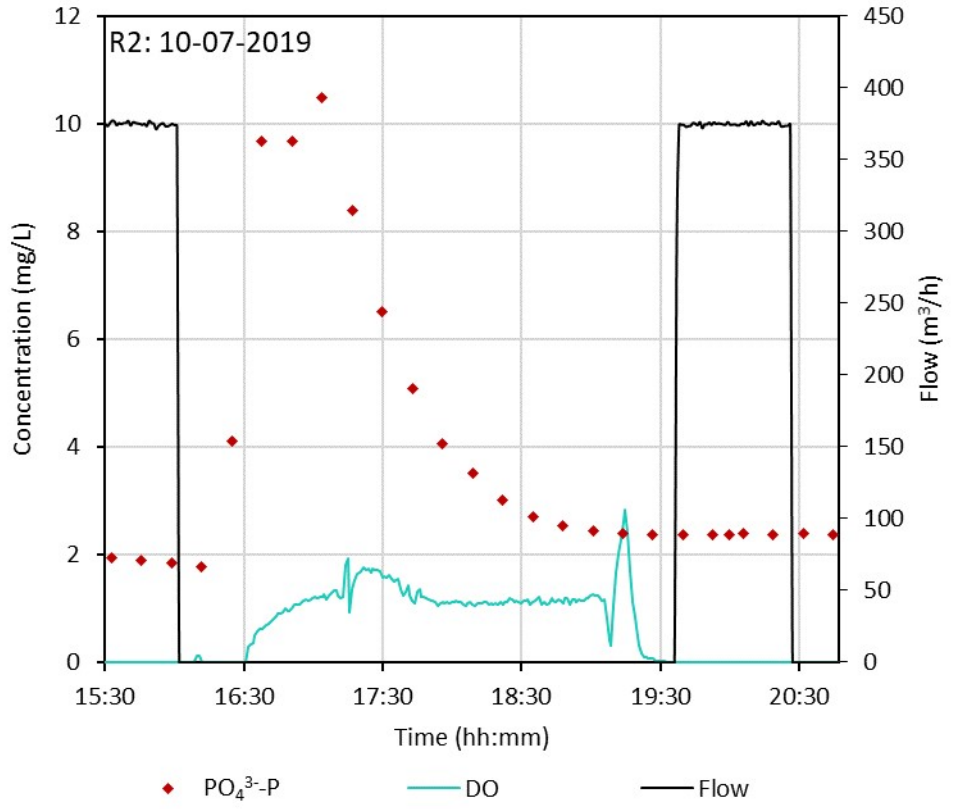

Figure S16. Online cycle data of phosphate and DO concentration and flow in R2 from 10th July 2019.

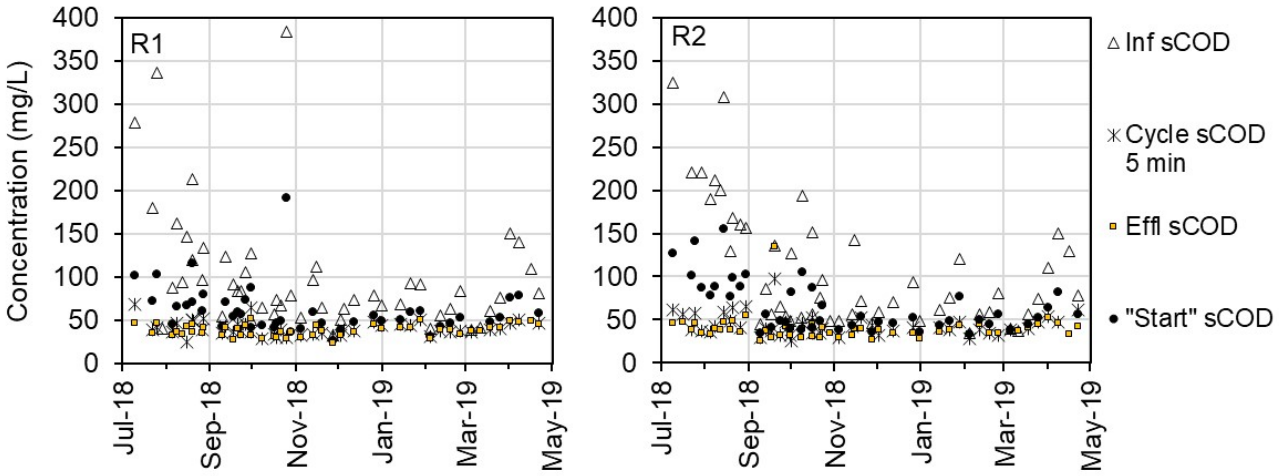

Figure S17. Concentration of soluble COD in R1 and R2 in the influent, after 5 minutes of aeration and effluent, as well as a calculated theoretical concentration at the start of aeration if no uptake during feeding would occur. The "Start" sCOD was calculated as follows: COD_{start} = ($COD_{influent}$ * exchange-ratio) + ($COD_{effluent}$ * (1-exchange-ratio)).

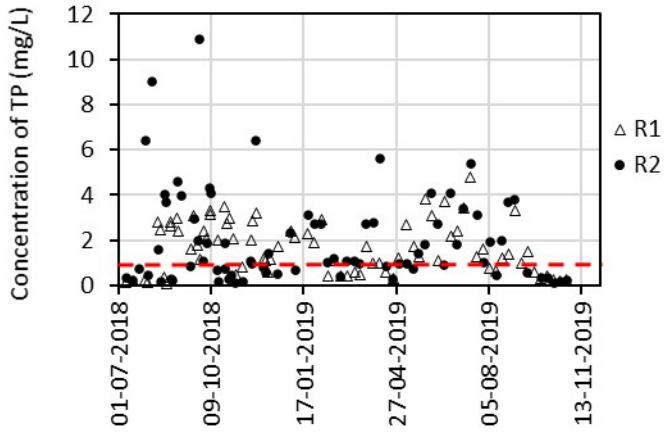

Figure S18. Effluent concentration of TP for R1 (triangles) and R2 (circles). The dashed line marks the effluent limit of 1 mg TP/L.

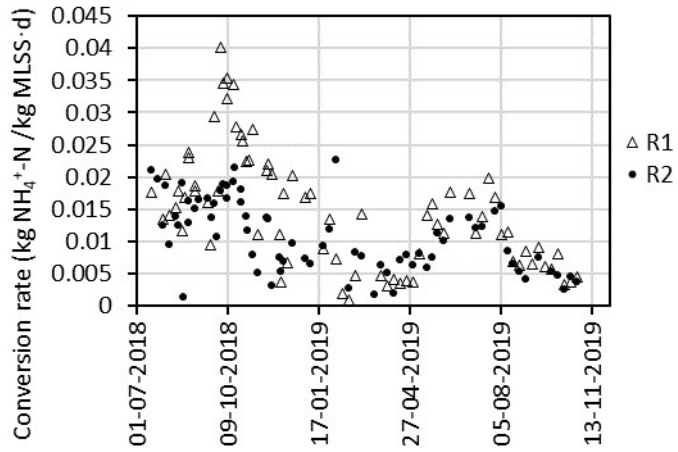

Figure S19. Specific conversion rates of ammonium for R1 and R2.

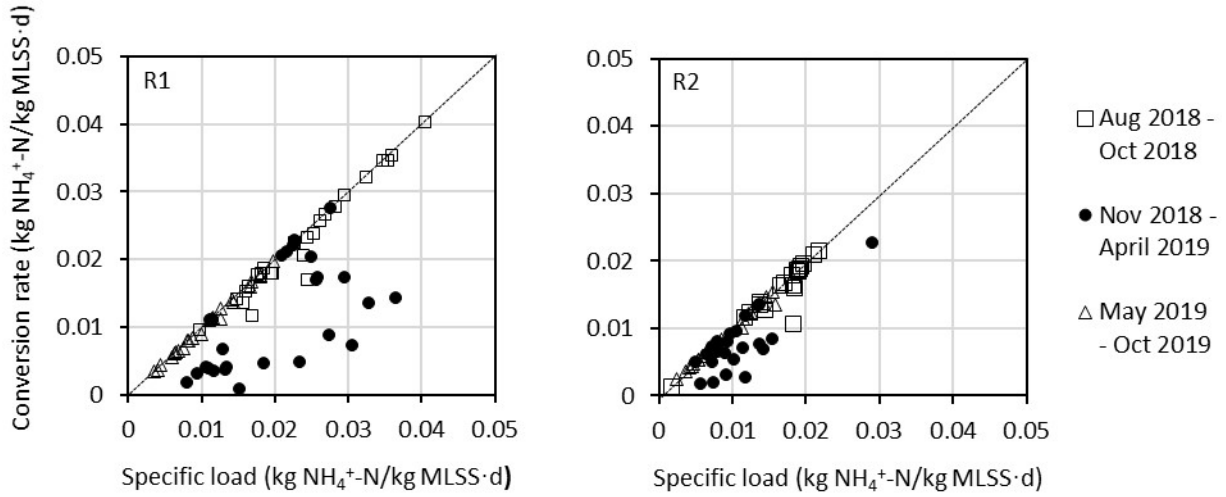

Figure S20. The specific conversion rate plotted against the specific load of ammonium for R1 (left) and R2 (right). Time periods are separated as follows: August to October 2018, November 2018 to April 2019 and May to October 2019.

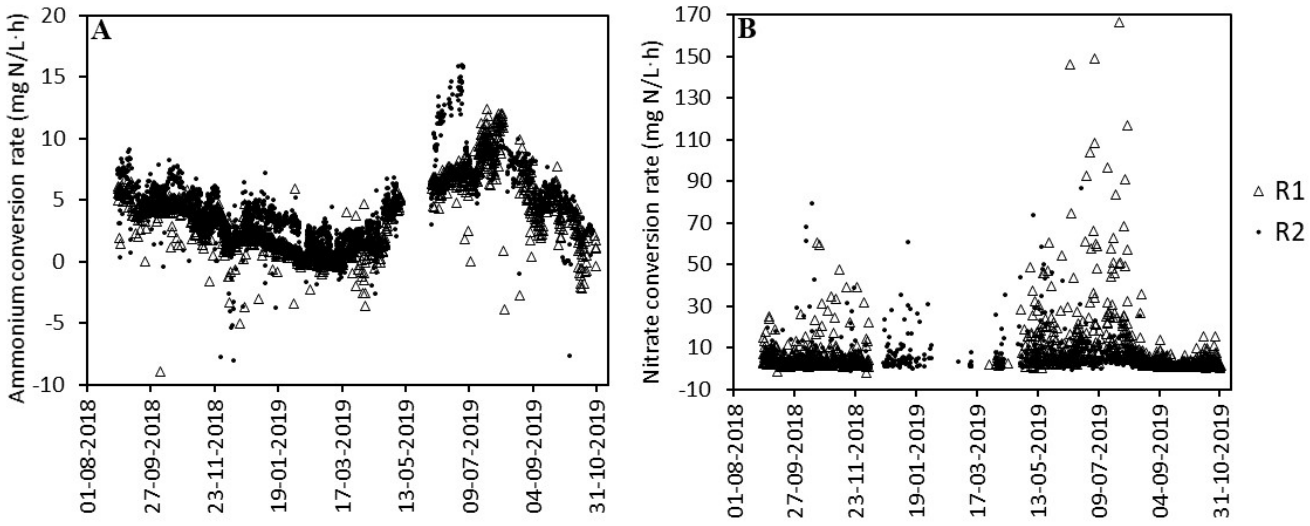

Figure S21. The conversion rates of ammonium- (A) and nitrate nitrogen (B).

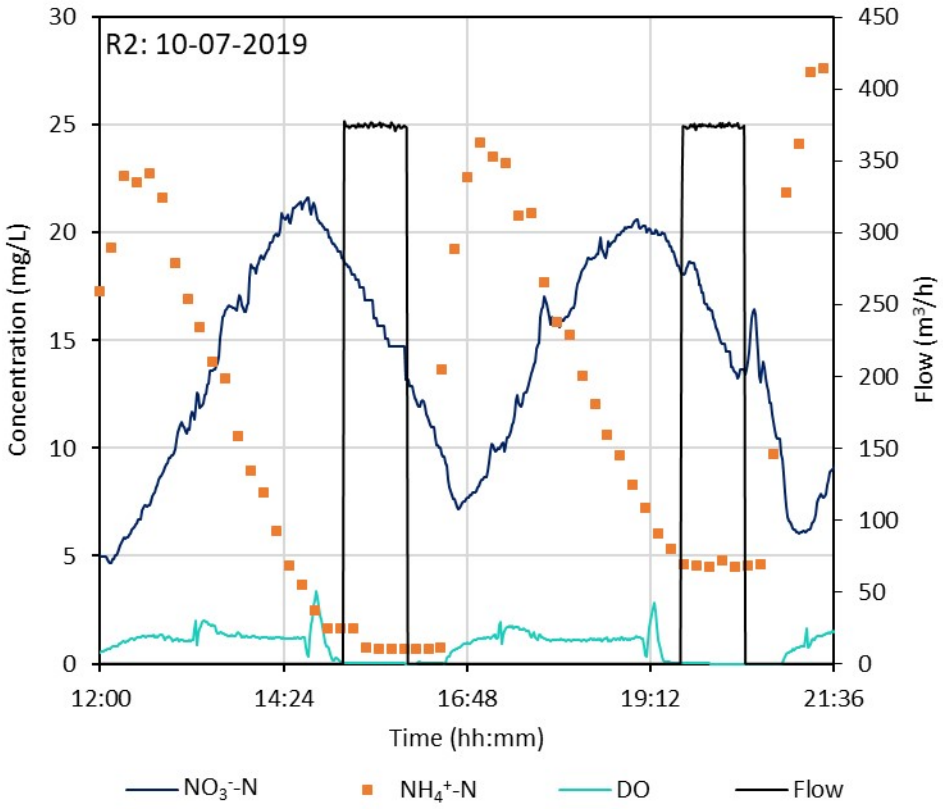

Figure S22. Online cycle data from R2 on the 10th of July 2019. The phosphate-phosphorus analyser was out of operation.

References

1. G. R. Crocetti, P. Hugenholtz, P. L. Bond, A. Schuler, J. r. Keller, D. Jenkins and L. L. Blackall, Identification of polyphosphate-accumulating organisms and design of 16S rRNA-directed probes for their detection and quantitation, *Applied and environmental microbiology*, 2000, **66**, 1175-1182.
2. M. S. Dueholm, K. S. Andersen, S. J. McIlroy, J. M. Kristensen, E. Yashiro, S. M. Karst, M. Albertsen and P. H. Nielsen, Generation of comprehensive ecosystem-specific reference databases with species-level resolution by high-throughput full-length 16S rRNA gene sequencing and automated taxonomy assignment (AutoTax), *MBio*, 2020, **11**, e01557-01520.
3. S. J. McIlroy, T. Nittami, E. Kanai, J. Fukuda, A. M. Saunders and P. H. Nielsen, Re-appraisal of the phylogeny and fluorescence in situ hybridization probes for the analysis of the C ompetibacteraceae in wastewater treatment systems, *Environmental microbiology reports*, 2015, **7**, 166-174.
4. H. Sanguin, A. Herrera, C. Oger-Desfeux, A. Dechesne, P. Simonet, E. Navarro, T. M. Vogel, Y. Moënne-Loccoz, X. Nesme and G. L. Grundmann, Development and validation of a prototype 16S rRNA-based taxonomic microarray for Alphaproteobacteria, *Environmental Microbiology*, 2006, **8**, 289-307.
5. M. Lukumbuzya, J. M. Kristensen, K. Kitzinger, A. Pommerening-Röser, P. H. Nielsen, M. Wagner, H. Daims and P. Pjevac, A refined set of rRNA-targeted oligonucleotide probes for in situ detection and quantification of ammonia-oxidizing bacteria, *Water Research*, 2020, **186**, 116372.
6. S. Lücker, J. Schwarz, C. Gruber-Dorninger, E. Spieck, M. Wagner and H. Daims, *Nitrotoga*-like bacteria are previously unrecognized key nitrite oxidizers in full-scale wastewater treatment plants, *ISME J.*, 2015, **9**, 708-720.
7. H. Daims, J. L. Nielsen, P. H. Nielsen, K.-H. Schleifer and M. Wagner, In situ characterization of Nitrospira-like nitrite-oxidizing bacteria active in wastewater treatment plants, *Applied and environmental microbiology*, 2001, **67**, 5273-5284.
8. J. R. Liu and R. J. Seviour, Design and application of oligonucleotide probes for fluorescent in situ identification of the filamentous bacterial morphotype Nostocoida limicola in activated sludge, *Environmental Microbiology*, 2001, **3**, 551-560.
9. R. Wehrens, H. Putter and L. M. Buydens, The bootstrap: a tutorial, *Chemometrics and intelligent laboratory systems*, 2000, **54**, 35-52.